RSC Advances

PAPER

View Article Online
View Journal | View Issue

Cite this: *RSC Adv.*, 2021, **11**, 22556

Low-fouling CNT-PEG-hydrogel coated quartz crystal microbalance sensor for saliva glucose detection†

Shiwen Wang,[ab] Guanjiang Liu,[b] Bei Yang,[b] Zifeng Zhang,[b] Debo Hu,[b] Chenchen Wu,[b] Yaling Qin,[b] Qian Dou,*[b] Qing Dai[b] and Wenping Hu*[a]

Saliva glucose detection based on a quartz crystal microbalance (QCM) sensor has emerged as a promising tool and a non-invasive diagnostic technique for diabetes. However, the low glucose concentration and strong protein interference in the saliva hinder the QCM sensors from practical applications. In this study, we present a robust and simple anti-fouling CNT-PEG-hydrogel film-coated QCM sensor for the detection of saliva glucose with high sensitivity. The CNT-PEG-hydrogel film consists of two layers; the bottom base PBA-hydrogel film is designed to recognize the glucose while the top CNT-PEG layer is used to restrict protein adsorption and improve the biocompatibility. Our results show that this CNT-PEG-hydrogel film exhibited a 10-fold enhancement on the detection limit compared to the PBA-hydrogel. Meanwhile, the adsorption of proteins on the surface of the CNT-PEG-hydrogel film, including bovine serum albumin (BSA), mucin (MUC), and fibrinogen (FIB), were reduced by 99.1%, 77.8%, and 83.7%, respectively. The CNT-PEG-hydrogel film could detect the typical saliva glucose level (0–50 mg L^{-1}) in 10% saliva with a good responsivity. To sum up, this new tool with low-fouling film featuring high stability, specificity, and selectivity holds great potential for non-invasive monitoring of saliva glucose in human physiological levels.

Received 12th April 2021
Accepted 14th June 2021

DOI: 10.1039/d1ra02841c

rsc.li/rsc-advances

Introduction

Diabetes is the most common endocrine disease often accompanied by complications such as periodontitis, kidney failure, blindness, *etc.*[1–4] So far, no definite cure has been developed, and continuous monitoring of blood glucose is needed to help doctors guide patients' treatment plans. The diagnostic methods for blood glucose detection are predominantly based on analyzing finger blood, venous blood, and intercellular fluid, which are all invasive.[5] Over the last decade, scientists have been trying to develop non-invasive methods for detecting glucose in sweat,[6] tears,[7] urine,[8] or saliva.[9,10] Among these specimens, saliva is an attractive alternative to blood, as its collection is inexpensive, and the method is completely non-invasive.[11] In addition, saliva glucose levels have been demonstrated to be positively correlated with blood glucose levels.[12]

Saliva glucose level is approximately 5–10 mg L^{-1} for healthy people, and above 10 mg L^{-1} in diabetic patients.[13,14] Since these concentration levels are only 1–10% of that found in blood, its detection requires platforms with extremely high sensitivity. Recent years have seen an increasing interest in using quartz crystal microbalances (QCMs) as biosensors for health monitoring, including antibody testing, glucose level monitoring, and others.[15–18] QCM is a mass sensor with a high accuracy that can realize specific rapid recognitions of various biomolecules when modified with different specially designed sensing materials.[19–24] For example, phenylboronic acid hydrogel (PBA-hydrogel) films have been respectively fabricated and immobilized onto the QCM electrodes to recognize glucose molecules. These films can provide boric acid sites that can bind with the glucose to trigger the frequency response of QCM.[15,16,25] Compared to traditional glucose-sensitive films, PBA-hydrogel offer higher sensitivity and accuracy. However, human saliva contains various proteins with much higher levels compared to glucose.[26,27] These proteins are indistinguishably adsorbed by the glucose-sensitive films, seriously interfering with the sensing-films/biomarkers interactions. To circumvent these limitations, a host of anti-fouling materials have been developed to resist protein adsorption. Those commonly-applied anti-fouling materials include poly(ethylene glycol) (PEG) and its derivatives,[28–30] zwitterionic materials,[31] bovine serum albumin (BSA),[32] peptides,[33] and other candidates (*e.g.*,

[a]*Tianjin Key Laboratory of Molecular Optoelectronic Sciences, Department of Chemistry, School of Sciences, Tianjin University, Tianjin, 300072, China. E-mail: huwp@tju.edu.cn*

[b]*Division of Nanophotonics, CAS Key Laboratory of Standardization and Measurement for Nanotechnology, CAS Center for Excellence in Nanoscience, National Center for Nanoscience and Technology, Beijing 100190, P. R. China. E-mail: douq@nanoctr.cn; Tel: +86-010-82545720*

† Electronic supplementary information (ESI) available. See DOI: 10.1039/d1ra02841c

hyaluronic acid (HA),[34] polyoxazoline,[35] *etc.*). Compared to these antifouling materials, PEG and its derivatives are some of the most accessible and adopted materials, which tend to hydrate and form a hydrophilic surface that generates a large entropic penalty by releasing and displacing its bound water so as to resist the non-specific adsorption of proteins.[30,36,37] Over the years, tremendous efforts have been made to optimize the sensing films, especially to design various anti-fouling brushes. For example, PEG coating has been designed as a simultaneous anti-fouling layer together with an antibody-sensing layer to detect insulin in 50% serum.[38] Nevertheless, great care has to be taken when designing and fabricating the anti-fouling PEG brushes, especially its packed density, since large steric hindrance may appear for densely packed brushes that significantly impede target molecules from transferring to the underlying sensing films and affect the sensitivity.[39,40] However, if the brushes are too sparsely arranged, their ability to form a stable hydration layer may be so greatly impaired that no significant performance of protein resistance can be achieved. To address these issues, new strategies have focused on designing anti-fouling films that can resist the non-specific adsorption of protein and allow access to glucose transferring simultaneously.

In this study, an innovative strategy that incorporates carbon nanotubes (CNT) decorated with PEG brushes coated onto the base PBA-hydrogel (CNT-PEG-hydrogel) film was designed to improve the glucose sensitivity and protein resistance at the same time. The CNTs were selected since they possess a huge surface-to-volume ratio that can immobilize the PEG brushes.[41] Meanwhile their porous structures provide adequate pathways for glucose transport. In addition, they are highly stable in both chemical and physical properties. All these qualities make CNTs the perfect solution for improving glucose sensitivity and protein resistance. The fabricated low-fouling CNT-PEG-hydrogel film consists of two layers, a bottom base glucose-sensitive PBA-hydrogel film and the topmost porous anti-fouling CNT-PEG coating. The testing results have shown that this combination possesses high sensitivity to glucose and superior ability to tolerate protein. In brief, this study presents a new strategy for improving the anti-fouling properties and the specificity of glucose-sensitive QCM sensors.

Results and discussion

Preparation of the CNT-PEG-hydrogel coated QCM electrode

CNT-PEG-hydrogel was successfully immobilized on the QCM electrode surface *via* a facile three-step method. Firstly, an adequate scheme is of great importance to achieve high loading of immobilized anti-fouling materials. CNT-COOH was used to load the PEG brushes as many as possible. The activation of carboxylate groups of CNT-COOH to form succinimidyl ester was achieved using EDC/NHS. NH_2–PEG–NH_2 was then immobilized to the CNT-COOH, forming CNT-PEG nanotubes (Fig. 1a). After the subsequent rinsing with redistilled water, an amount of ether structures was seen on the surface of CNT-PEG coating. Subsequently, the quartz electrode was first cleaned with piranha solution and rinsed with ultrapure water to eliminate organic substances, the double bond can be modified by immersing electrode into mixed solution of maleic anhydride (100 mg) and *N*,*N*′-dimethylformamide (5 mL) for 12 h. Then the QCM electrode was immersed in the prepolymer solution (consisting of AM, 3-PBA, and BIS) for 1 h. PBA hydrogel film was obtained by pressing-assisted UV exposure on the upper side of the QCM electrode (Fig. 1b).[42] Finally, CNT-PEG dispersion was spin-coated on the PBA-hydrogel film and allowed to form CNT-PEG-hydrogel.

PBA-hydrogel consists of AM, BIS, and 3-PBA. AM is used as a common monomer for hydrogel materials, BIS contains double bonds at both ends and is used as a cross-linking agent, and 3-PBA contains phenylboronic acid groups that enable the recognition of glucose. Phenylboronic acid has long-term stability in aqueous buffers and exists in two forms in an aqueous solution: in a negatively charged dissociated state and an uncharged non-dissociated state. The boronic acid groups are in equilibrium between the non-dissociated and the dissociated form. Non-dissociated is a flat triangle and forms an unstable complex with glucose, while a dissociated state has a tetrahedral structure and can form cyclic lactones with glucose forming glucose–boronate complex.[16] Therefore, the PBA-hydrogel could form a stable complex with glucose. Furthermore, PEG could resist nonspecific protein adhesion through the entropic penalty of releasing and displacing bound water from the hydrophilic PEG surface.[30,43] In addition, CNT-COOH has a unique structure with a high surface area that can immobilize PEG brushes and provide adequate pathways that permit glucose molecules to transfer and bind with the bottom PBA-hydrogen film. Therefore, the CNT-PEG-hydrogel film features stability, high specificity, selectivity, and excellent anti-fouling properties, rendering the QCM sensor highly sensitive and accurate to detect and monitor saliva glucose.

Characterization of PBA-hydrogel and CNT-PEG-hydrogel coated electrode

The morphology of CNT-COOH and CNT-PEG were characterized using TEM (HT-7700). The CNT-PEG shows a typical CNT hollow fibber shape. Compared to the neat CNT-COOH, an amorphous layer was seen in CNT-PEG, which denotes that the PEG is successfully grafted on the CNT-COOH nanotube (Fig. 2a and b). Raman spectra (Renishaw) approved the hybrid carbon of CNT-COOH and CNT-PEG. An increase in the D band's peak intensity ratio over the G band (D/G) from 0.31 to 0.60 (Fig. 2c) was found for CNT-PEG. The increased D/G value indicates that the chemical reaction occurs at the sp^2 hybrid carbon of CNT-COOH to form sp^3 hybrid carbon.

The contact angle measurement is useful in evaluating surface macroscopic properties, such as surface energy and hydrophilicity (wettability).[44,45] If the substrate has relatively high surface energy, the liquid will wet the solid surface showing a small contact angle; conversely, low surface energy results in a large contact angle.[46] In this study, the contact angle measurements were used to further examine the hydrophilicity properties of the PBA-hydrogel and CNT-PEG-hydrogel. PEG brushes can improve the aqueous surface wettability and form

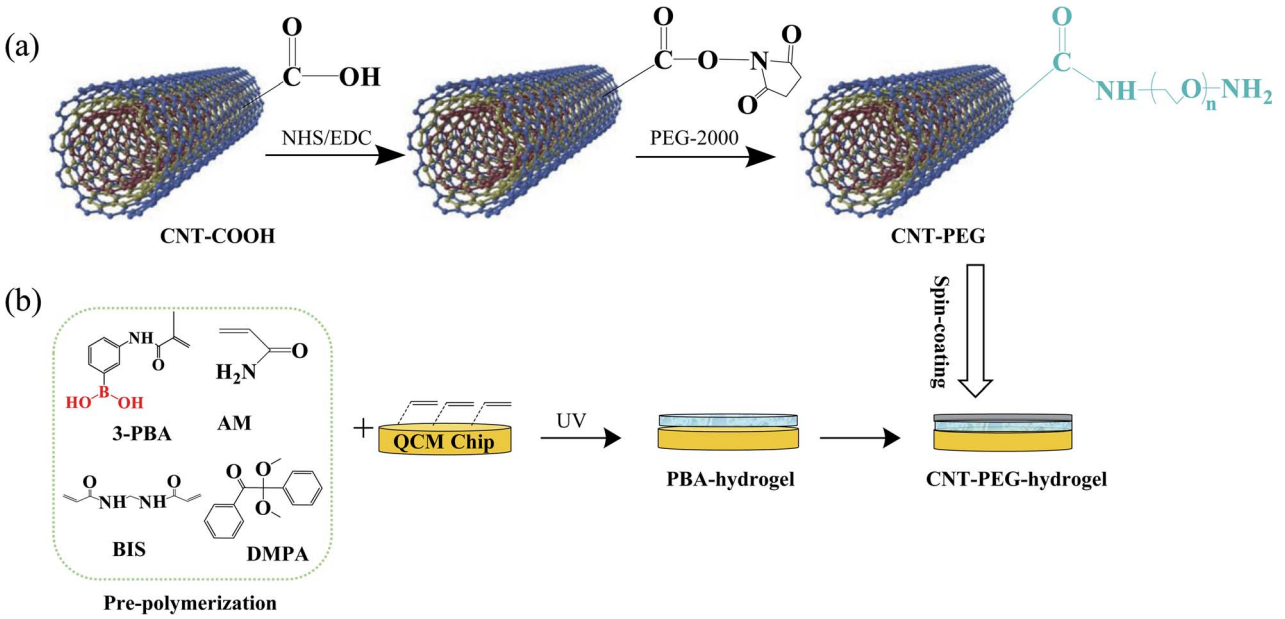

Fig. 1 (a) The synthesis procedure for the CNT-PEG. (b) The quartz chip was coated with CNT-PEG-hydrogel.

a stable hydration layer, which is beneficial for resisting protein adsorption and improving the diffusion of soluble glucose through to PBA-hydrogel.[47] The water contact angle of CNT-PEG-hydrogel was 49.0° ± 2.3° (Fig. 2g), half of the PBA-hydrogel (79.5° ± 2.8°, Fig. 2d). These results demonstrated that CNT-PEG-hydrogel could form a stable hydration layer, and hydrophilicity was improved.

To better understand these enhanced glucose-sensing properties, we characterized the porosity and topography of the PBA-hydrogel and CNT-PEG-hydrogel using SEM and AFM. For the PBA-hydrogel with a smooth surface (Fig. 2d, e and S2a†), the surface roughness of the PBA-hydrogel-coated electrode was RMS = 3.99 ± 1.08 nm (Fig. S2a†), and the thickness of the PBA-hydrogel films was 322 ± 24 nm (Fig. 2d). After coating CNT-PEG onto the surface of the PBA-hydrogel, the surface appeared uneven, and CNT-PEG staggered on the surface of hydrogel (Fig. 2g and h). Moreover, the surface roughness was increased to RMS = 44.06 ± 14.4 nm (Fig. S2b†), and the thickness of the CNT-PEG-hydrogel was increased to 754 ± 14 nm (Fig. 2g), which further proved that the CNT-PEG nanocomposite coating was successfully fixed onto the surface of PBA-hydrogel. In addition, the PBA-hydrogel displayed many regular holes 8–10 nm in diameter that can provide enough glucose transfer pathways (Fig. 2e). In contrast, CNT-PEG-hydrogel displayed 5–10 nm that can filter out some proteins (the diameter ranged from 2 nm to tens of nanometers[48]) and allow the glucose (the diameter is 0.36 nm (ref. 49)) through to the PBA-hydrogel (Fig. 2h).

X-ray photoelectron spectroscopy (XPS, ESCALAB250Xi) was used to examine the surface composition of the CNT-PEG-hydrogel (Fig. 2f). The presence of PBA-hydrogel was confirmed by the high-resolution XPS of B 1s located at ~191.5 eV (Fig. S2†).[25] Moreover, the detailed XPS data of different samples are shown in Table S1.† This indicates that the CNT-PEG was successfully attached to the surface of the PBA-hydrogel.

Fourier Transform Infrared Spectroscopy (FTIR) was used to verify the chemical structure of the materials (Fig. 2i, S4a and b†). The broad mode centered at ~3200 cm^{-1} was predominately due to the N–H stretching motions of the amide group. The predominant modes at ~2940 cm^{-1} were due to the symmetric and asymmetric stretching motions of the methylene groups. The PBA-hydrogel revealed two peaks at ~1660 cm^{-1} that were predominately due to C=O and N–H bending. The band centered at ~1344 cm^{-1} was due to vibrational modes involving B–O stretching motions (Fig. S3b†).[42] The appearance of these modes indicated that the PBA-hydrogel was successfully grown on the surface of the QCM electrode. After PEG was fixed on the CNT-COOH, there was a strong absorption peak around ~1110 cm^{-1}, which was predominately due to the C–O–C stretching motion (Fig. S4a†). These modes and intensities indicated the introduction of an ether bond (PEG), while it could also be inferred that CNT-PEG was successfully synthesized.

Glucose sensitivity of CNT-PEG-hydrogel coated QCM sensor

QCM sensor can provide a sensitive means for direct label-free detection of biomarkers by modifying different sensitive materials on the QCM electrode. In this study, CNT-PEG-hydrogel and PBA-hydrogel-coated QCM sensors were applied to detect glucose concentrations. Firstly, the stability of the PBA-hydrogel and CNT-PEG-hydrogel was evaluated in PBS. When the QCM electrodes were immersed in PBS for nearly 2 h, the frequency shift fluctuations (ΔF) were only ~4.6 Hz and ~1.0 Hz (Fig. 3a and e), respectively, suggesting that the rigid CNT-PEG coating improves the stability of the sensor.

As it was reported,[27,50] the detection limit of the PBA-hydrogel and CNT-PEG-hydrogel was based on a QCM sensor that

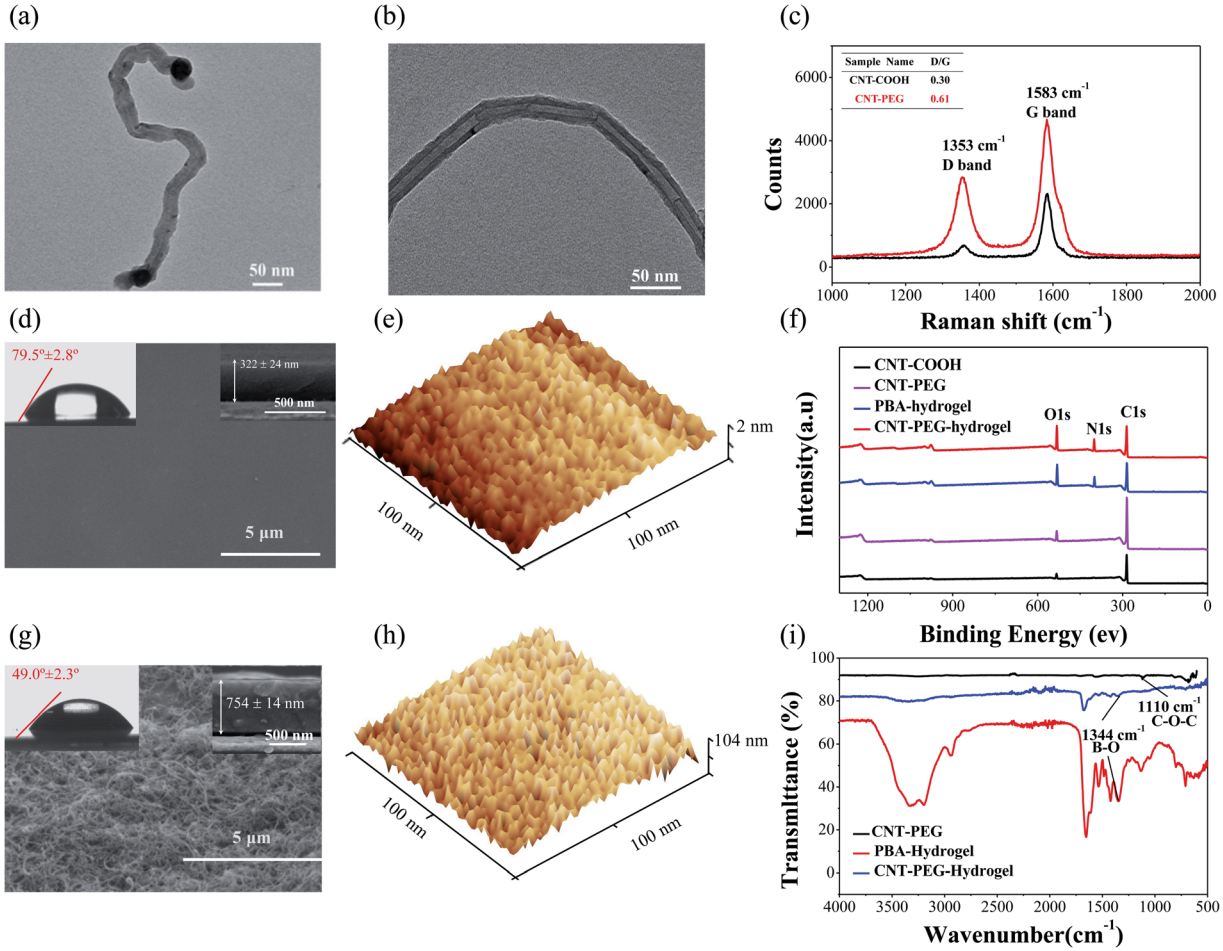

Fig. 2 (a) TEM micrographs of CNT-COOH. (b) TEM micrographs of CNT-PEG. (c) Raman spectra of CNT-COOH and CNT-PEG. (d) Water contact angles and SEM images of PBA-hydrogel films. (e) AFM images of the PBA-hydrogel films. (f) XPS spectra of CNT-COOH, CNT-PEG, PBA-hydrogel, and CNT-PEG-hydrogel. (g) Water contact angles and SEM images of CNT-PEG-hydrogel films. (h) AFM images of the CNT-hydrogel films. (i) FTIR spectra of the CNT-PEG nanocomposite coating, PBA-hydrogel films, and CNT-PEG-hydrogel films.

gradually increased the glucose concentration. When the concentration increased to 5 mg L^{-1}, ΔF had a noticeable decrease (LOD = 5 mg L^{-1}) (Fig. 3b). For CNT-PEG-hydrogel coated QCM, ΔF had an apparent decrease when the glucose concentration increased to 0.5 mg L^{-1} (LOD = 0.5 mg L^{-1}) (Fig. 3f). Because CNT-PEG was able to bind a significant amount of water molecules *via* hydrogen bonding and form a hydration layer, it led to higher swelling and porosity.[47] So, the detection limit of the CNT-PEG-hydrogel film-coated QCM sensor was decreased after coating CNT-PEG on the PBA-hydrogel.

The detection medium's pH value has a vital role in the binding ability of the PBA-hydrogel and CNT-PEG-hydrogel. After increasing the pH, the number of charged species increases. Consequently, the hydrogel swells due to the Donnan effect.[51] Moreover, the higher pH promoting ionization of boric acid and increasing the number of glucose molecules that bind to boric acids stimulate the PBA-hydrogel and CNT-PEG-hydrogel swelling. With alkaline enhancements, the boronic acid groups have a stronger binding affinity to diols in an alkaline environment. As shown in Fig. 3c and g, when the glucose concentration gradually increases from 0 to 50 mg L^{-1}, the absolute value of ΔF increases rapidly. Glucose binding of PBA-hydrogel and CNT-PEG-hydrogel at pH 6.8 results in a slight frequency shift value of ΔF increase was proportional to the glucose concentrations at different pH. For CNT-PEG-hydrogel, the relevant coefficient between glucose concentration and ΔF was 0.9883 (pH = 6.8), 0.9951 (pH = 7.2), and 0.9976 (pH = 7.5), respectively (Fig. 3g). Thus, CNT-PEG-hydrogel adequately encompassed the range of glucose concentration in physiological conditions, and the dynamic range of the PBA-hydrogel coated, and CNT-PEG-hydrogel was broad enough to cover the typical range of saliva glucose.[52] Interestingly, compared with the PBA-hydrogel, the ΔF of CNT-PEG-hydrogel showed obvious changes and increased by ~1.5 times.

Phenylboronic acid and its derivatives can covalently bind to glucose and reversibly form a boric acid diester.[53] To assess the reversibility of glucose binding to the PBA functionalized hydrogel, we exposed a QCM electrode modified with PBA-hydrogel and CNT-PEG-hydrogel to the buffer solution (pH = 7.5) without or with 50 mg L^{-1} glucose. As illustrated by the data

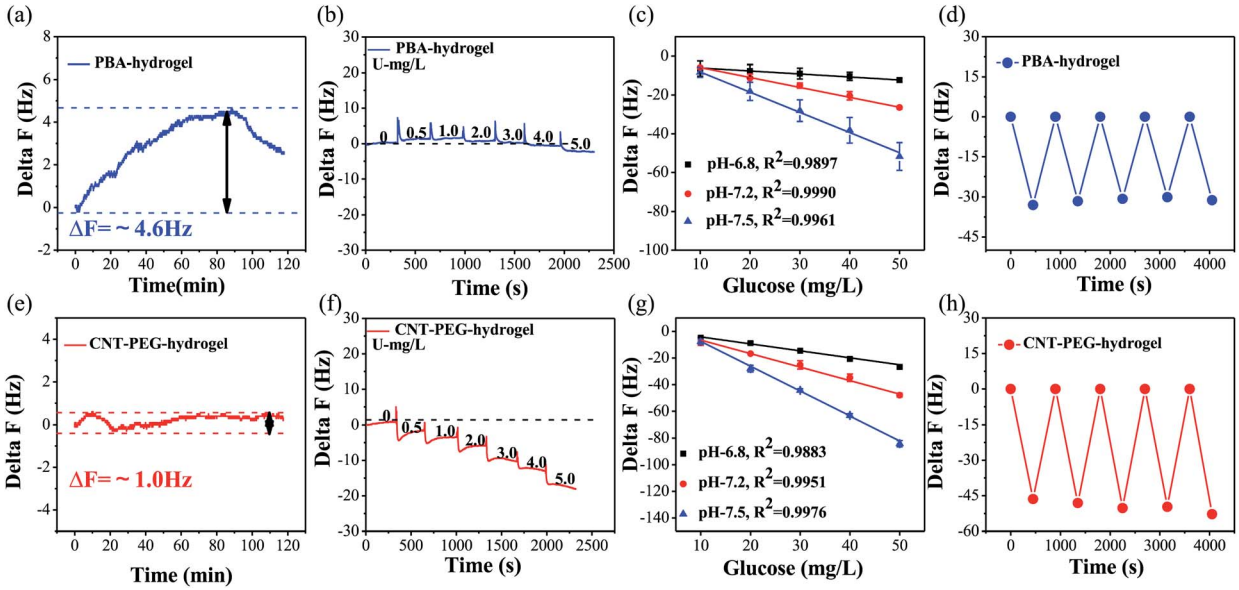

Fig. 3 (a) The stability of PBA-hydrogel film in PBS solution at pH = 7.5. (b) The low detection limit of the PBA-hydrogel film. (c) Response of the PBA-hydrogel film at different pH values (6.8–7.5). (d) Repeatability of PBA-hydrogel film coated QCM sensor. (e) The stability of CNT-PEG-hydrogel film in PBS solution at pH = 7.5. (f) The low detection limit of CNT-PEG-hydrogel film. (g) Response of the CNT-PEG-hydrogel film at different pH values (6.8–7.5). (h) Repeatability of CNT-PEG-hydrogel film coated QCM sensor.

in Fig. 3d and h, both the PBA-hydrogel and CNT-PEG-hydrogel coated QCM response to five alternating exposures to 50 mg L^{-1} glucose and 0 mg L^{-1} glucose in PBS solution was constant (Fig. 3h). Moreover, as listed in Table S2,† the relative standard deviations (RSD) of ΔF for PBA-hydrogel and CNT-PEG-hydrogel coated sensors were 3.2% and 5.1% ($n = 5$). Considering the blood glucose sensors variances of disposable and continuous monitoring systems typically range from 3 to 10%,[54] the repeatability of both PBA-hydrogel and CNT-PEG-hydrogel film was acceptable.

Protein resistance of CNT-PEG-hydrogel coated QCM sensor

The composition of saliva is complex and contains a variety of proteins. These proteins can be adsorbed and hinder the QCM sensor from maintaining its sensing functionality.[43] CNT-PEG coating tends to form a stable hydration layer that generates entropic penalty by releasing and displacing its bound water, thus restricting nonspecific adsorption of proteins.[39] To improve the ability of protein resistance, the CNT-PEG nanocomposite was coated on the surface of the PBA-hydrogel. We prepared different thickness of the CNT-PEG-hydrogel. The thicknesses of the CNT-PEG-hydrogel (such as 383 ± 15 nm, 559 ± 32 nm, and 754 ± 14 nm) were proportional to the CNT-PEG concentration (250 mg L^{-1}, 500 mg L^{-1}, 100 mg L^{-1}) (Fig. S5†). At the appropriate thickness, the CNT-PEG coating forms a hydration layer and improves aqueous surface wettability, which, in turn, improves the anti-fouling properties while enhancing glucose transfer to the sensing films. According to the results, the CNT-PEG-hydrogel film's protein-resistant properties improved as the thickness increased, and the thickness had no obvious effect on the glucose-sensitive (Fig. S5†). When the thickness of CNT-PEG approaches 754 ± 14 nm, it can anti-foul but also improve glucose transfer to the sensing films. The protein-resistant properties of the CNT-PEG-hydrogel and PBA-hydrogel, the adsorption of BSA, MUC, and FIB were measured by QCM sensor (Fig. 4a). Compared with PBA-hydrogel, the adsorption of BSA, MUC, and FIB could be reduced by nearly 99.1%, 77.8%, and 83.7%, respectively, indicating the CNT-PEG-hydrogel has excellent protein resistance.

Apart from proteins, some small molecules in human saliva, *e.g.* uric acid (UA), L-cysteine (L-Cys), L-glutathione (GSH) and creatinine (CRE), also influenced the accuracy of the test results.[55] As shown in the Fig. 4b and Table S4,† the responding frequency of UA (100 mg L^{-1}), L-Cys (100 mg L^{-1}), GSH (100 mg L^{-1}), and CRE (100 mg L^{-1}) was −6.5 ± 2.2 Hz, 9.0 ± 4.9 Hz, 10.8 ± 2.6 Hz, −5.4 ± 2.6 Hz, respectively. While the responding frequency of 100 mg L^{-1} glucose was −161.0 ± 19.0 Hz. This result indicates small molecules disturbance to measurements of glucose detection can be ignored.

To evaluate the sensitivity of the CNT-PEG-hydrogel coated sensor to glucose in real human saliva, a moderate amount of glucose was spiked into the 10% saliva ($V_{\text{mixed saliva}} : V_{\text{pH-7.5 PBS}} = 9 : 1$). At 50 mg L^{-1} glucose, the ΔF of the CNT-PEG-hydrogel was ~80 Hz in 10% saliva (Fig. 4d), which is an approach to the ΔF of PBS. Due to the nonspecific adsorption of protein, the ΔF of PBA-hydrogel was ~201 Hz in 10% saliva (Fig. 4c), almost 2.5 times more than CNT-PEG-hydrogel. The CNT-PEG-hydrogel film-coated sensor had a good linear relationship between glucose concentration and ΔF, ($R^2 = 0.9990$) in 10% saliva (Fig. S8†). Moreover, as listed in Table S3,† the relative standard deviations (RSD) of CNT-PEG-hydrogel coated sensors were 9.1%, 11.2%, and 8.2% respectively ($n = 5$). This result indicates

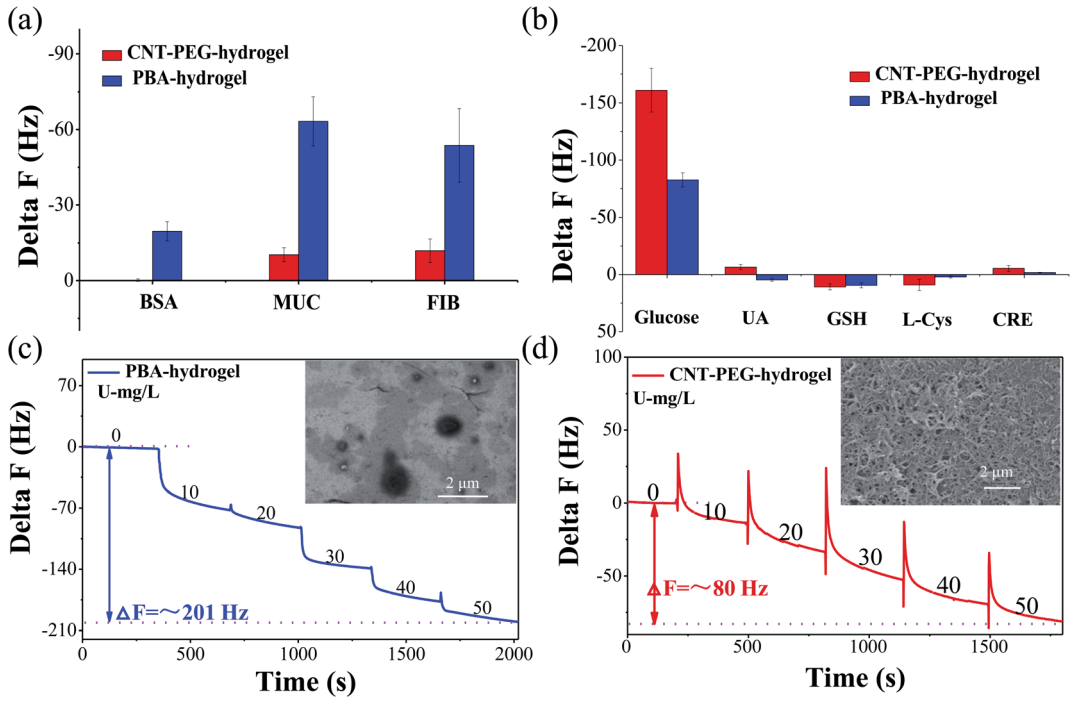

Fig. 4 (a) Adsorption of BSA (500 mg L^{-1}), MUC (500 mg L^{-1}), FIB (500 mg L^{-1}) on the CNT-PEG-hydrogel and PBA-hydrogel film-coated QCM sensor. (b) Response of small molecules (GSH, CRE, UA, AA and L-Cys, 100 mg L^{-1}) and glucose on the CNT-PEG-hydrogel and PBA-hydrogel film-coated QCM sensor. (c) Response of glucose in diluted saliva (10%) by the PBA-hydrogel film. (d) Response of glucose in diluted saliva (10%) by the CNT-PEG-hydrogel film.

that the CNT-PEG-hydrogel film-coated QCM sensor has an acceptable reproducibility in 10% saliva.

To further verify the protein-resistive properties of the CNT-PEG-hydrogel, we carried out SEM imaging of CNT-PEG-hydrogel and PBA-hydrogel after incubating with saliva for 24 h. As shown in Fig. 4c, some cracks appeared, and impurities were adsorbed on the surface of PBA-hydrogel. By contrast, impurities on the surface of CNT-PEG-hydrogel were nearly unobservable (Fig. 4d). These results indicated that the CNT-PEG-hydrogel possesses excellent resistance to nonspecific adsorption of protein compared to PBA-hydrogel. These data also demonstrated that the CNT-PEG-hydrogel film-coated QCM sensor holds significant potential for non-invasive monitoring of glucose in saliva.

As shown in Table S5,† to epitomize the advantage of the QCM glucose sensor, some detection methods were also compared. The advantages of CNT-PEG-hydrogel film-coated QCM sensor over other detection methods like Field Effect Transistor (FET) sensors are excellent anti-fouling properties, glucose sensitivity, and time saving.[49]

Conclusions

A new type of low-fouling CNT-PEG-hydrogel film-coated QCM sensor, which was designed, fabricated, and tested to detect the saliva glucose level, showed notable performances in both protein resistance and glucose sensitivity. This designed CNT-PEG-hydrogel film consists of two layers as a topmost porous CNT-PEG coating and a base PBA-hydrogel film at the bottom. The former layer tends to form a stable hydration layer that restricts the adhesion of protein; meanwhile, its porous framework provides adequate pathways that permit small glucose molecules to transfer to the bottom PBA-hydrogel film. The testing results showed that the glucose sensitivity of this CNT-PEG-hydrogel film was enhanced by nearly 10-folds compared to that of the PBA-hydrogel film, and the nonspecific adsorption of BSA, MUC, and FIB was reduced by nearly 99.1%, 77.8%, and 83.7%, respectively. Hence, CNT-PEG-hydrogel enables glucose detection (0–50 mg L^{-1}) in 10% saliva with a good response, which can be seen as a considerable improvement for the existing glucose-sensitive QCM sensors. This design film features easy preparation, stability, high specificity, and selectivity, thus having great potential for non-invasive monitoring of human glucose levels.

Materials and methods

Materials

N,*N*-Methylenebisacrylamide (BIS, 98%) was purchased from Singapore Harm Chemical Reagent Co., Ltd. 3-Aminophenylboronic acid (3-PBA, 98%), 1-ethyl-3-(3-dimethylaminopropyl)carbodiimide (EDC, 98%), *N*-hydroxysuccinimide (NHS, 98%), 3-aminopropyltriethoxysilane (APTES, 98%) were bought from Alfa Aesar Chemicals Co., Ltd. Acrylamide (AM, 98.5%) were from Xilong Chemical Industry Incorporated Co. Ltd. 2,2-Dimethoxy-1,2-diphenylethanone (DMPA, 98%) were from Tokyo Chemical Industry. Carboxylic multi-walled carbon nanotubes (CNT-COOH, >95%) were

purchased from Shanghai Macklin Biochemical Co., Ltd, and the content of –COOH was about 3.9%. Amine–PEG–amine (NH_2–PEG–NH_2, >98%, MW = 2000) was acquired from Beijing HWRK Chem Co., Ltd. Fibrinogen (FIB), mucin (MUC), and bovine serum albumin (BSA) were purchased from Shanghai Yuanye Biotechnology Co. Ltd. Analytically pure reagents (glucose, ethanol, dimethyl sulfoxide, *N*,*N*-dimethylformamide, H_2SO_4 (98%), H_2O_2 (30%), sodium phosphate dibasic dodecahydrate and potassium dihydrogen phosphate) were used for carrying out the experiments.

Saliva samples

Saliva samples were provided by the project "early identification, early diagnosis and cutting point of diabetes risk factors" (2016YFC1305700). All participants were between 18–82 years old and they provided written informed consent. The donors fasted for 8 h prior to collecting samples. Participation in these studies was voluntary, and the medical ethics committee of Jiangsu Provincial Center for Disease Control and Prevention (JSJK2017-B003-02). China has approved the study protocols. To reduce the impact of differences in individual saliva content and acquire enough saliva samples, we mixed the saliva samples that originate from multiple people. Before the measurement, ion chromatography was used to detect the concentration of glucose in the mixed saliva. Only the glucose concentration of the mixed saliva is $\leq$1 mg L^{-1} that can be applied for glucose detection.

Saliva collection tubes (Salivette) were used to collect "fasting saliva". The tubes were centrifuged for 10 min at 4000 rpm to extract saliva. Saliva aliquots were stored at −20 °C before analysis to maintain their biological characteristics.

Instrumentation

Glucose and anti-fouling tests were performed using a quartz crystal microbalance (QCM 200, Stanford Research Systems). The surface topography and thickness of the hydrogel were obtained by scanning electron microscope (SU-8200). Atomic force microscopy (AFM, M8-HR) was used to determine the morphology and roughness of the hydrogel. Hydrophilicity was measured by using a fully automatic contact angle measuring instrument (DSA-100). The functional groups of the materials were determined using a Fourier-transform infrared spectrometer (Nicolet 560). X-ray photoelectron spectroscopy (XPS, ESCALAB250X) was used to examine the surface composition of the CNT-COOH, CNT-PEG, PBA-hydrogel, and CNT-hydrogel film. The forces applied during the preparation of hydrogel were realized using a lab-built pressure machine. Ultraviolet polymerization was achieved using a UV lamp (the wavelength is 365 nm, and the maximum power is 3 W). The CNT-PEG coating was formed by Spin-coater (KW-4B, Beijing Teesside Case Electronics Co., Ltd.).

Surface modification of the QCM electrode

The QCM electrodes were sonicated for 10 min within piranha solution (H_2SO_4 (98% w/w) and H_2O_2 (30% w/w) in a volume ratio of 7 : 3). Then, they were sonicated with ethanol and acetone for 10 min to remove the protective impurities. The processed electrodes were washed with redistilled water and dried with N_2, and then immersed in a mixed solution of 3-aminopropyltriethoxysilane (100 μL) and ethanol (50 mL) at room temperature. After 12 h, the QCM electrodes were rinsed with ethanol and subsequently dried with N_2. The dried electrodes were immersed in a mixed solution of maleic anhydride (500 mg) and *N*,*N*-dimethylformamide (25 mL) for 12 h.[42] Finally, the treated electrodes were rinsed with ethanol and dried with N_2.

Preparation of PBA-hydrogel film

The preparation of PBA-hydrogel film was prepared as follows: (1) 5 mol L^{-1} prepolymer solution was prepared, consisting of 35.07% 3-PBA, 3.14% BIS, 56.56% AM, and 5.23% DMPA dimethyl sulfoxide; (2) 25 μL of the pre-polymerization solution was dropped onto a quartz plate. The electrode was placed face down on the pre-polymerization solution and pressed with reasonable force. The crystal plate was irradiated with a UV lamp (λ = 365 nm) for 1 h, after which it was placed in distilled water for about 1 h to automatically detach the hydrogel-coated QCM sensor from the working solid substrate-crystal plate. (3) The PBA-hydrogel-coated electrode was rinsed with redistilled water.

Preparation of CNT-PEG nanocomposite

Firstly, 50 mg of multiwalled CNT-COOH was sonicated in a bath sonicator (80 W) for 30 min within 15 mL of phosphate buffered saline (PBS, 15 mL, pH = 7.0), which enabled the CNT-COOH to disperse uniformly. Then, the CNT-COOH could be functionalized using carbodiimide chemistry; 100 mg EDC, and 125 mg NHS, which were sonicated in the PBS solution for 30 min at 30 °C. Subsequently, 100 mg NH_2–PEG–NH_2 was added into PBS mixture solution and stirred for 24 h at 30 °C. The CNT-PEG was recovered by centrifugation, and the pellet was washed with deionized water to remove PEG excess. A black residue (CNT-PEG) was obtained after drying under a vacuum.

Preparation of CNT-PEG-hydrogel film

The CNT-PEG nanocomposite dispersions was prepared by mixing 10 mL EtOH/H_2O (V : V = 3 : 1) solution with 10 mg CNT-PEG and sonicating for 5 min. The PBA-hydrogel-coated QCM electrode was then rinsed with deionized water to remove impurities and subsequently dried with N_2. Next, the CNT-PEG dispersions were directly spin-coated (at a speed of 1000 rpm, 30 s) on the PBA-hydrogel's surface. Finally, the CNT-hydrogel was obtained after drying under a vacuum for 24 h at 45 °C, after which the CNT-PEG-hydrogel film was thoroughly rinsed in deionized water.

The evaluation of glucose detection capacity and anti-fouling performance

The CNT-PEG-hydrogel and PBA-hydrogel-coated QCM electrodes were rinsed with deionized water and installed in the flow cell of the QCM-200 system. Subsequently, the sample

solution was pumped into the flow cell continuously using a peristaltic pump, and the frequency of the electrode was recorded by data acquisition software. When voltage is applied to a quartz crystal, causing it to oscillate at a specific frequency, the change in mass on the quartz surface is related to the change in the oscillating crystal frequency. The frequency shift (ΔF), which is equal to the frequency of the glucose sample minus the blank sample's frequency was used to estimate the glucose concentrations. If ΔF was stabilized, the glucose detection capacity and anti-fouling performance of the CNT-hydrogel and PBA-hydrogel coated QCM sensor were evaluated. The glucose detection capacity of the sensor was evaluated under different glucose concentration from 0 to 50 mg L^{-1}, which was gradually pumped into the flow cell with a flow rate of $\sim$100 μL s^{-1}. And the ΔF with each glucose concentration was recorded for 5 min. The effect of pH was investigated by conducting measurement at different pH values from 6.8 to 7.5, 500 mg L^{-1} different kinds of proteins (FIB, MUC, BSA) have been measured according to the above procedure.

Conflicts of interest

There are no conflicts to declare.

Acknowledgements

This work was supported by the National Key Research and Development Program of China (2016YFA0201600), the National Natural Science Foundation of China (U2032206), and Science and Technology Service Network Project (STS Program) of the Chinese Academy of Sciences (KFJ-STS-ZDTP-063).

Notes and references

1 A. K. Wooton and L. Melchior, *The Nurse Practitioner*, 2020, **45**, 31–32.
2 G. Basta, P. Montanucci and R. Calafiore, *J. Diabetes Invest.*, 2021, **12**, 301–309.
3 S. Ma, S. Li, R. Lv, X. Hou, S. Nie and Q. Yin, *J. Diabetes Invest.*, 2020, **11**, 1295–1302.
4 G. C. Singh, M. Ahmed, M. Zaid and S. Hasnain, *Mol. Genet. Genomic Med.*, 2020, **8**, e1147.
5 G. G. Kang, N. Francis, R. Hill, D. Waters and A. B. Santhakumar, *Int. J. Mol. Sci.*, 2019, **21**, 140.
6 E. V. Karpova, E. V. Shcherbacheva, A. A. Galushin, D. V. Vokhmyanina, E. E. Karyakina and A. A. Karyakin, *Anal. Chem.*, 2019, **91**, 3778–3783.
7 S. Kim, H. J. Jeon, S. Park, D. Y. Lee and E. Chung, *Sci. Rep.*, 2020, **10**, 8254.
8 A. K. Wooton and L. Melchior, *The Nurse Practitioner*, 2020, **45**, 24–31.
9 Q. Liu, Y. Liu, F. Wu, X. Cao, Z. Li, M. Alharbi, A. N. Abbas, M. R. Amer and C. Zhou, *ACS Nano*, 2018, **12**, 1170–1178.
10 E. Vargas, H. Teymourian, F. Tehrani, E. Eksin, E. Sanchez-Tirado, P. Warren, A. Erdem, E. Dassau and J. Wang, *Angew. Chem., Int. Ed.*, 2019, **58**, 6376–6379.
11 K. Uppu, S. Sahana, G. P. Madu, A. A. Vasa, S. Nalluri, K. J. Raghavendra and N. Marwah, *International Journal of Clinical Pediatric Dentistry*, 2018, **11**, 71–78.
12 V. Gupta and A. Kaur, *J. Oral Maxillofac. Pathol.*, 2020, **24**, 187.
13 S.-J. Luis, M.-L. Alfredo, O. Velia, E. M. Ivan and D. Rocio, *Sensors*, 2018, **18**, 1071.
14 T. Arakawa, Y. Kuroki, H. Nitta, P. Chouhan, K. Toma, S. I. Sawada, S. Takeuchi, T. Sekita, K. Akiyoshi and S. Minakuchi, *Biosens. Bioelectron.*, 2016, 106–111.
15 Q. Dou, D. B. Hu, H. K. Gao, Y. M. Zhang, A. K. Yetisen, H. Butt, J. Wang, G. J. Nie and Q. Dai, *RSC Adv.*, 2017, **7**, 41384–41390.
16 Z. Zhang, Q. Dou, S. Wang, D. Hu, X. Guo, B. Liao, Z. Zhao, H. Liu and Q. Dai, *J. Mater. Chem. C*, 2020, **8**, 9655–9662.
17 Z. M. Dong, L. Cheng, P. Zhang and G. C. Zhao, *Analyst*, 2020, **145**, 3329–3338.
18 M. Hussain, *RSC Adv.*, 2015, **5**, 54963–54970.
19 B. Ding, X. F. Wang, J. Y. Yu and M. R. Wang, *J. Mater. Chem.*, 2011, **21**, 12784–12792.
20 J. Y. Lim and S. S. Lee, *Anal. Methods*, 2020, **12**, 5103–5109.
21 M. Q. Yang and J. H. He, *RSC Adv.*, 2018, **8**, 22–27.
22 L. J. Chi, C. Xu, S. Y. Li, X. Y. Wang, D. P. Tang and F. Q. Xue, *Analyst*, 2020, **145**, 6111–6118.
23 R. Akter, C. K. Rhee and M. A. Rahman, *Biosens. Bioelectron.*, 2015, **66**, 539–546.
24 S. Akgonullu, D. Battal, M. S. Yalcin, H. Yavuz and A. Denizli, *Microchem. J.*, 2020, **153**, 104454.
25 C. Sugnaux and H. A. Klok, *Macromol. Rapid Commun.*, 2014, **35**, 1402–1407.
26 T. Riedel, S. Hageneder, F. Surman, O. Pop-Georgievski, C. Noehammer, M. Hofner, E. Brynda, C. Rodriguez-Emmenegger and J. Dostalek, *Anal. Chem.*, 2017, **89**, 2972–2977.
27 Q. Dou, S. W. Wang, Z. F. Zhang, Y. X. Wang, Z. P. Zhao, H. J. Guo, H. L. Liu and Q. Dai, *Nanoscale*, 2020, **12**, 19317–19324.
28 J. Sun, H. Tan, H. Liu, D. Jin, M. Yin, H. Lin, X. Qu and C. Liu, *Biomater. Sci.*, 2020, **8**, 6946–6956.
29 S. Sunoqrot, N. N. Mahmoud, L. H. Ibrahim, S. Al-Dabash, H. Raschke and R. Hergenroder, *ACS Biomater. Sci. Eng.*, 2020, **6**, 4424–4432.
30 K. X. Zhang, H. Huang, H. C. Hung, C. Leng, S. Wei, R. Crisci, S. Y. Jiang and Z. Chen, *Langmuir*, 2020, **36**, 2030–2036.
31 P. Kaner, A. V. Dudchenko, M. S. Mauter and A. Asatekin, *J. Mater. Chem. A*, 2019, **7**, 4829–4846.
32 A. Munoz-Calderon, D. Wehrendt, C. Cura, A. Gomez-Bravo, M. Abril, M. Giammaria, R. H. Lucero and A. G. Schijman, *Infect., Genet. Evol.*, 2020, **83**, 104328.
33 Y. Li, L. Wang, C. Ding and X. Luo, *Biosens. Bioelectron.*, 2019, **142**, 111553.
34 Y. Xia, V. Adibnia, C. Shan, R. Huang, W. Qi, Z. He, G. Xie, M. Olszewski, G. De Crescenzo, K. Matyjaszewski, X. Banquy and R. Su, *Langmuir*, 2019, **35**, 15535–15542.
35 G. Morgese, Y. Gombert, S. N. Ramakrishna and E. M. Benetti, *ACS Appl. Mater. Interfaces*, 2018, **10**, 41839–41848.

36 A. B. Kutikov and J. Song, *ACS Biomater. Sci. Eng.*, 2015, **1**, 463–480.
37 S. Lowe, N. M. O'Brien-Simpson and L. A. Connal, *Polym. Chem.*, 2015, **6**, 198–212.
38 M. Y. Xu, X. L. Luo and J. J. Davis, *Biosens. Bioelectron.*, 2013, **39**, 21–25.
39 S. Chen, L. Li, Z. Chao and Z. Jie, *Polymer*, 2010, **51**, 5283–5293.
40 I. Banerjee, R. C. Pangule and R. S. Kane, *Adv. Mater.*, 2011, **23**, 690–718.
41 S. Freddi, G. Drera, S. Pagliara, A. Goldoni and L. Sangaletti, *Analyst*, 2019, **144**, 4100–4110.
42 Q. Dou, Z. Zhang, Y. Wang, S. Wang, D. Hu, Z. Zhao, H. Liu and Q. Dai, *ACS Appl. Mater. Interfaces*, 2020, **12**, 34190–34197.
43 C. Jiang, G. X. Wang, R. Hein, N. Z. Liu, X. L. Luo and J. J. Davis, *Chem. Rev.*, 2020, **120**, 3852–3889.
44 B. Andreotti and J. H. Snoeijer, *Annu. Rev. Fluid. Mech.*, 2020, **52**, 285–308.
45 Z. Zhang, W. Wang, A. N. Korpacz, C. R. Dufour, Z. J. Weiland, C. R. Lambert and M. T. Timko, *Langmuir*, 2019, **35**, 12317–12325.
46 G. Lamour, A. Hamraoui, A. Buvailo, Y. J. Xing, S. Keuleyan, V. Prakash, A. Eftekhari-Bafrooei and E. Borguet, *J. Chem. Educ.*, 2010, **87**, 1403–1407.
47 K. Shah, D. Vasileva, A. Karadaghy and S. P. Zustiak, *J. Mater. Chem. B*, 2015, **3**, 7950–7962.
48 M. Kopp, S. Kollenda and M. Epple, *Acc. Chem. Res.*, 2017, **50**, 1383–1390.
49 C. Li, X. Chen, F. Y. Zhang, X. X. He, G. Z. Fang, J. F. Liu and S. Wang, *Anal. Chem.*, 2017, **89**, 10431–10438.
50 Z. F. Zhang, Q. Dou, S. W. Wang, D. B. Hu, B. Yang, Z. P. Zhao, H. L. Liu and Q. Dai, *Nanoscale*, 2020, **12**, 22787–22797.
51 A. Kim, S. Mujumdar and R. Siegel, *Chemosensors*, 2013, **2**, 1–12.
52 S. J. Luis, M. L. Alfredo, O. Velia, E. M. Ivan and D. Rocio, *Sensors*, 2018, **18**, 1071.
53 G. Ye and X. Wang, *Biosens. Bioelectron.*, 2011, **26**, 772–777.
54 A. Heller and B. Feldman, *Chem. Rev.*, 2008, **108**, 2482.
55 K. Ngamchuea, K. Chaisiwamongkhol, C. Batchelor-McAuley and R. G. Compton, *Analyst*, 2018, **143**, 777–783.